A Facile Approach for Graphdiyne Preparation in Atmosphere for Advanced Battery Anode

Zicheng Zuo *[,a], Hong Shang[a], Yanhuan Chen[a, b], Jiaofu Li[a, b], Huibiao Liu[a, b], Yongjun Li[a, b], and Yuliang Li *[,a, b]

[a] Beijing National Laboratory for Molecular Sciences (BNLMS), CAS Research/Education Center for Excellence in Molecular Sciences; CAS Key Laboratory of Organic Solids, Institute of Chemistry, Chinese Academy of Sciences, Beijing 100190, P. R. China
E-mail: ylli@iccas.ac.cn; zuozic@iccas.ac.cn

[b] University of Chinese Academy of Sciences, Beijing 100049, PR China

Characterization of GDY

The as-prepared samples is characterized by field emission scanning electron microscopy FESEM (Hitachi S-4800, FESEM) and transmission electron microscopy (JEM-2100F, TEM) for their morphology information without further treatments. Raman spectra is obtained using an NT-MDT NTEGRA Spectra system with the excitation from an Ar laser at 473 nm. All solid state ^{13}C-NMR analyses of GDY were performed in Bruker Avance AV III 400. The X-ray photoelectron spectroscopic (XPS) is recorded on ESCALab250Xi for analyzing the elementary information.

Electrochemical testing

For the Li/Na-ion anode tests, the slurry containing GDY (80%), super P (10%), and PVDF (10%) in 1-methyl-2-pyrrolidone (NMP) is uniformly coated on the cupper foil by doctor blade with the area loading of 1.5 mg/cm^2. After then, it is dried at 120 °C in a vacuum oven overnight. The as-prepared electrode is cut into small round pieces with the diameter of 1 centimeter. For the lithium-ion anode application, the electrolyte is 1 M $LiPF_6$ in ethylene carbonate and dimethyl carbonate (EC: DMC, 1:1 in volume), the separator is Celgard 2300 membrane, and lithium foil is used as counter electrode.

For the sodium-ion anode application, the electrolyte is 1 M $NaClO_4$ in propylene carbonate, the glass fiber is used as the separator, and the sodium foil is used as counter electrode. The cyclic voltammetry (CV) curves at different rate and electrochemical impedance spectra (EIS) are recorded by the CHI 660 D, and EIS is tested using a sinusoidal signal with amplitude of 10 mV over a frequency range from 100 000 to 0.1 Hz. Galvanostatic charge/discharge curves and long-time stability are both recorded in the LAND battery testing system.

The metal ion diffusion coefficient is obtained from the following equation:

$$I_p = 2.69 \times 10^5 n^{3/2} A D_{Li}^{1/2} v^{1/2} C_0$$

in which I_p is the peak current intensity, n is the electron transfer number per ion, A is the surface area, D_{Li} is the diffusion coefficient of active ion, v is the scanning rate, C_0 is the maximum Li ion concentration in the GDY materials.

Table S1. The conditions of prevailing carbon preparation

Materials	Production Condition	Ref.
Carbon Nanotube	Higher than 800 °C in inert atmosphere	[1]
Graphene	Higher than 1000 °C in inert atmosphere	[2,3]
Fullerence	Arc Discharge in inert atmosphere	[4]
Carbon Nitride	Higher than 450 °C in inert atmosphere	[5]
Amorphous Carbon	Higher than 800 °C in inert atmosphere	[6]
Diamond	1100 -3700 °C high pressure in inert atmosphere	[7,8]
Carbon Fiber	Higher than 700 °C	[9]
Porous carbon	Higher than 600°C in inert atmosphere	[10]
Pyrolytic Carbon	Higher than 700 °C in inert atmosphere	[11]
Onion Carbon	Higher than 1100 °C in inert atmosphere	[12,13]

This work	120 °C in air	

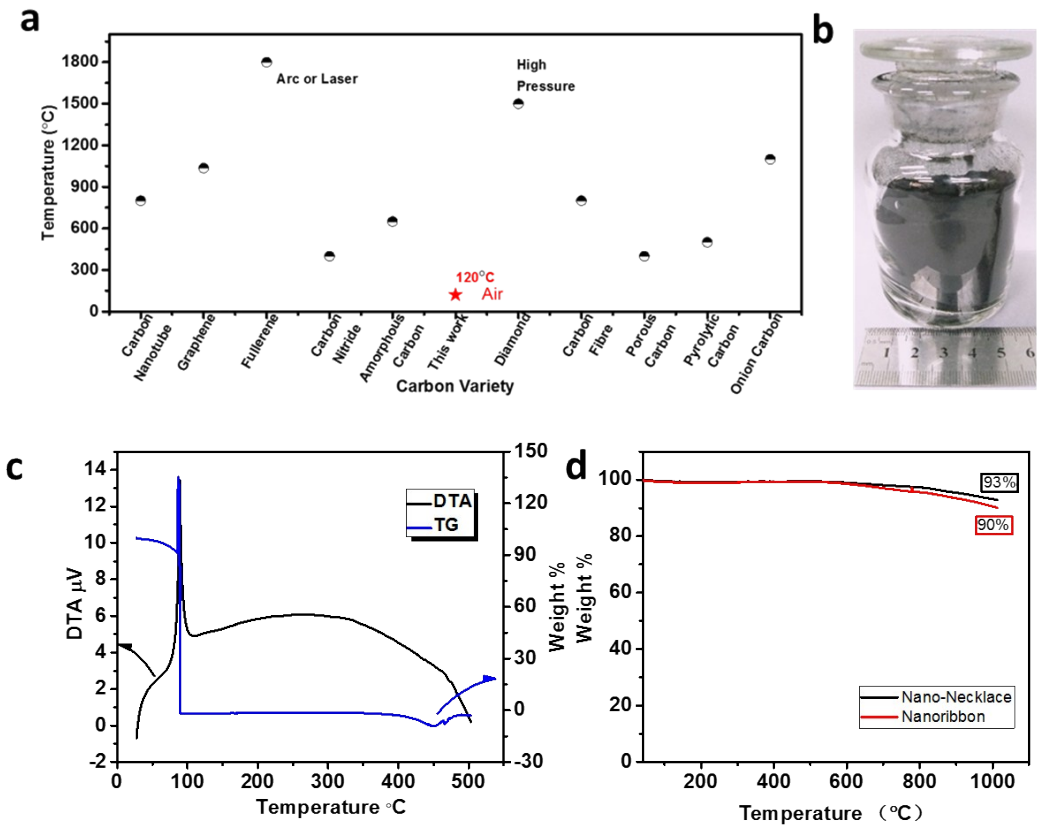

Figure S1.a) fabrication conditions of the prevailing all carbons reported (listed in Table S1); b) photo of large-scale GDY nanochain (3 gram); c) TG and DTG curves of HEB and d) the stability of the as-prepared GDY nanoribbon and nanochain.

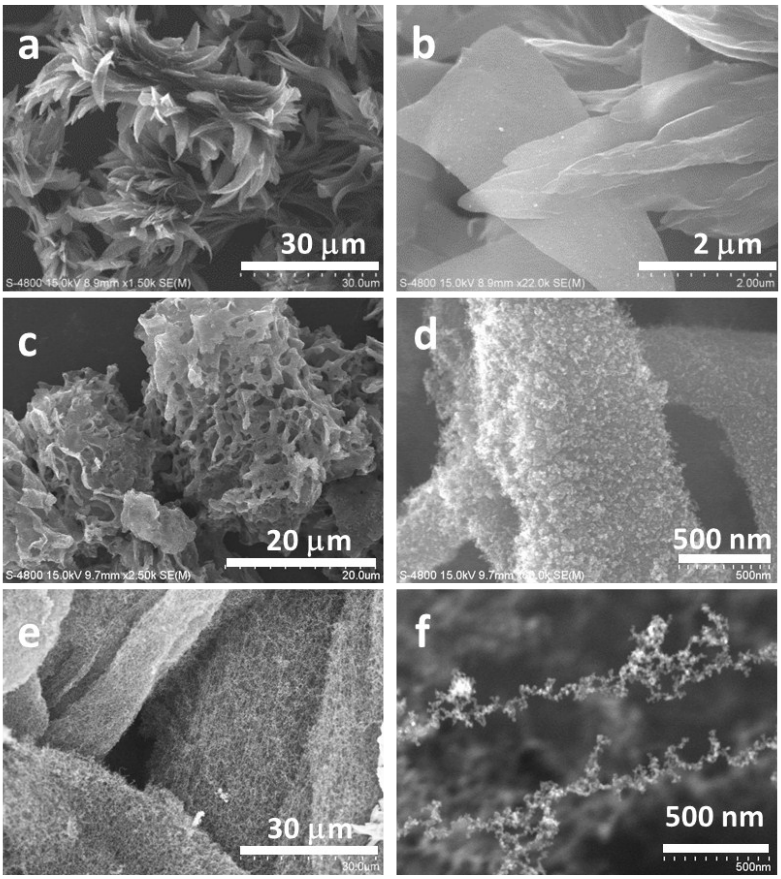

Figure S2. SEM images of GDY nanostructures. a), b) GDY ribbon under different magnification; c), d) 3D framework of GDY under different magnifications; e), f) GDY nanochains under different magnifications.

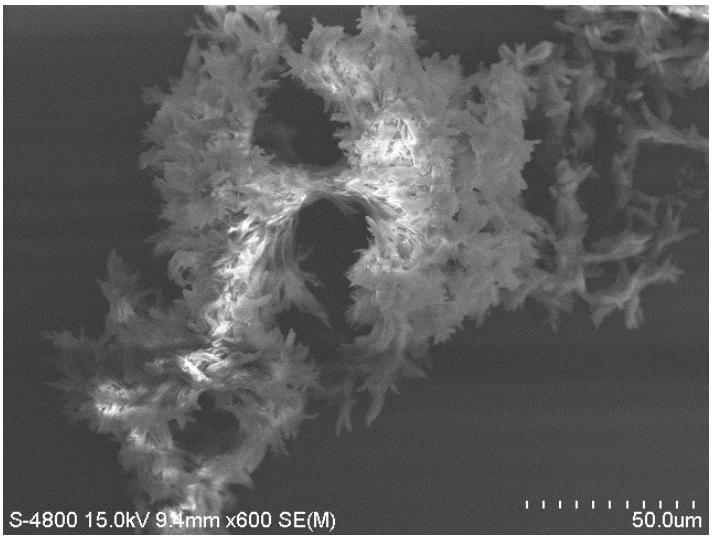

Figure S3. SEM of precursor HEB.

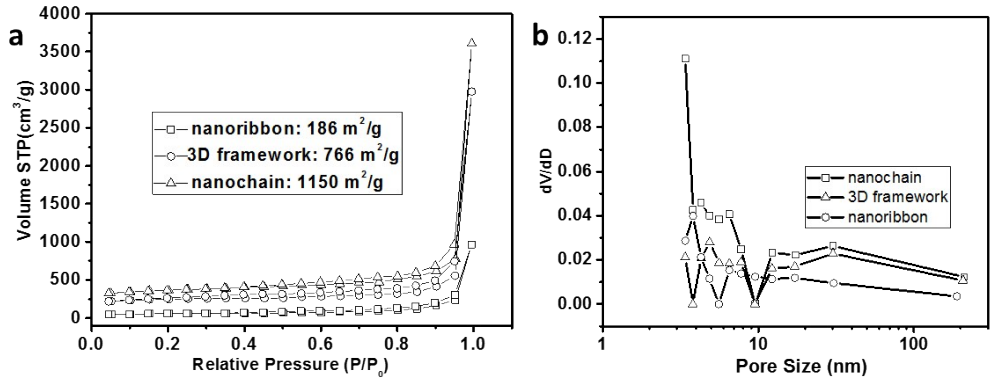

Figure S4. a) N_2 absorption/desorption curves and b) the pore size distribution of 2D nanoribbon, 3D framework, and 1D nanochain.

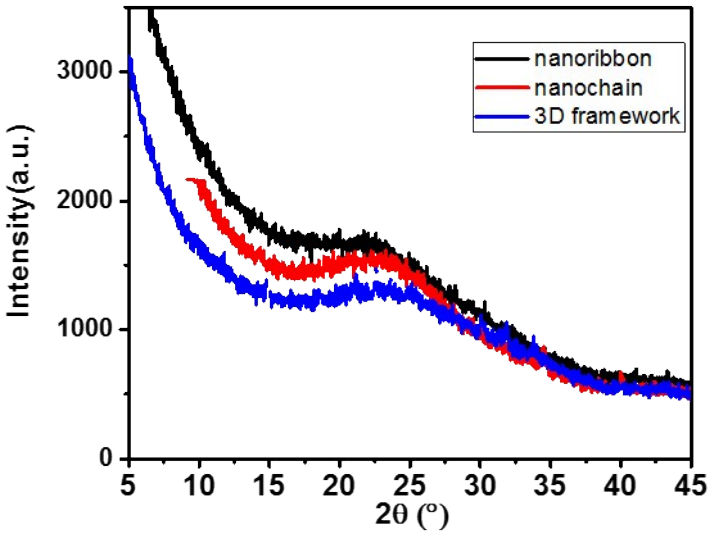

Figure S5. The XRD curves of as-prepared GDY samples.

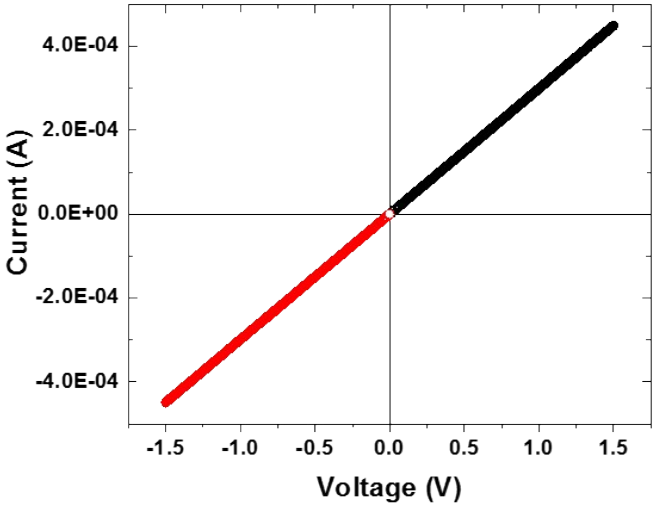

Figure S6. I-V curves of GDY electrode based on the nanochain.

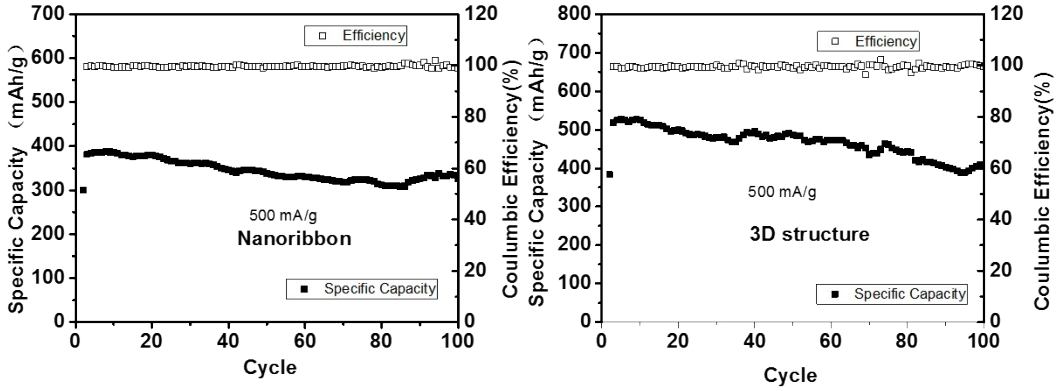

Figure S7. Long-term Stability of GDY nanoribbon and 3D framework.

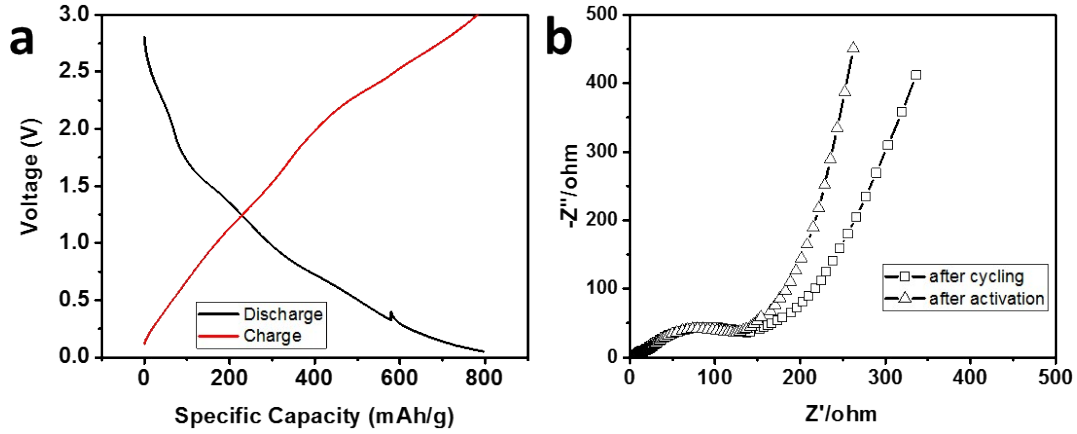

Figure S8. a) The charge/discharge curves of GDY nanochain at 50 mA/g after 500 cycles at a high rate testing in the lithium ion storage; b) the EIS change before and after cycling are illustrated.

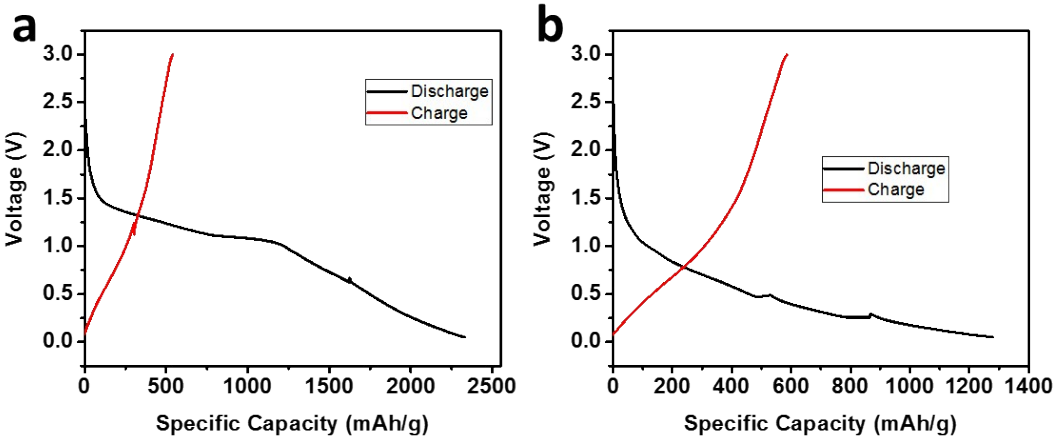

Figure S9. First charge-discharge curves of a) nanoribbon and b) 3D framework at 50 mA/g in the application of sodium-ion storage.

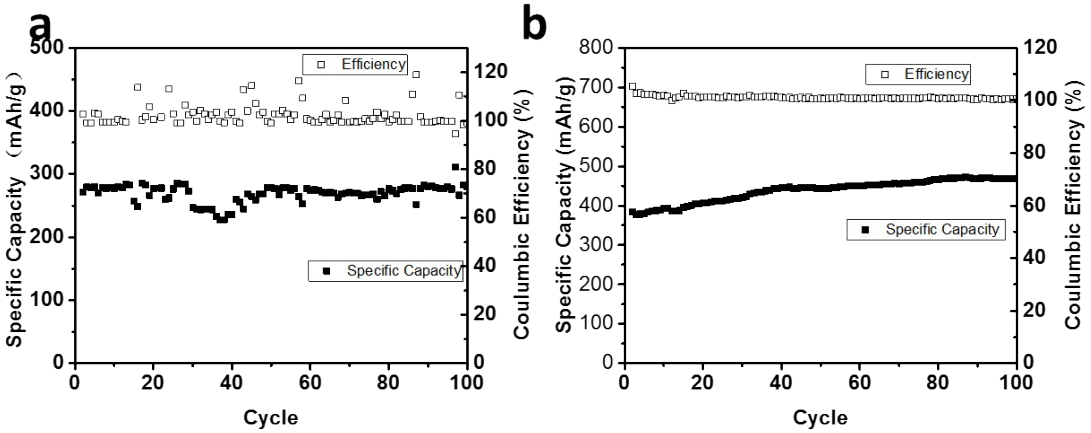

Figure S10. The long-term stability of a) 2D nanoribbon and b) 3D framework in the application of sodium-ion battery anode.

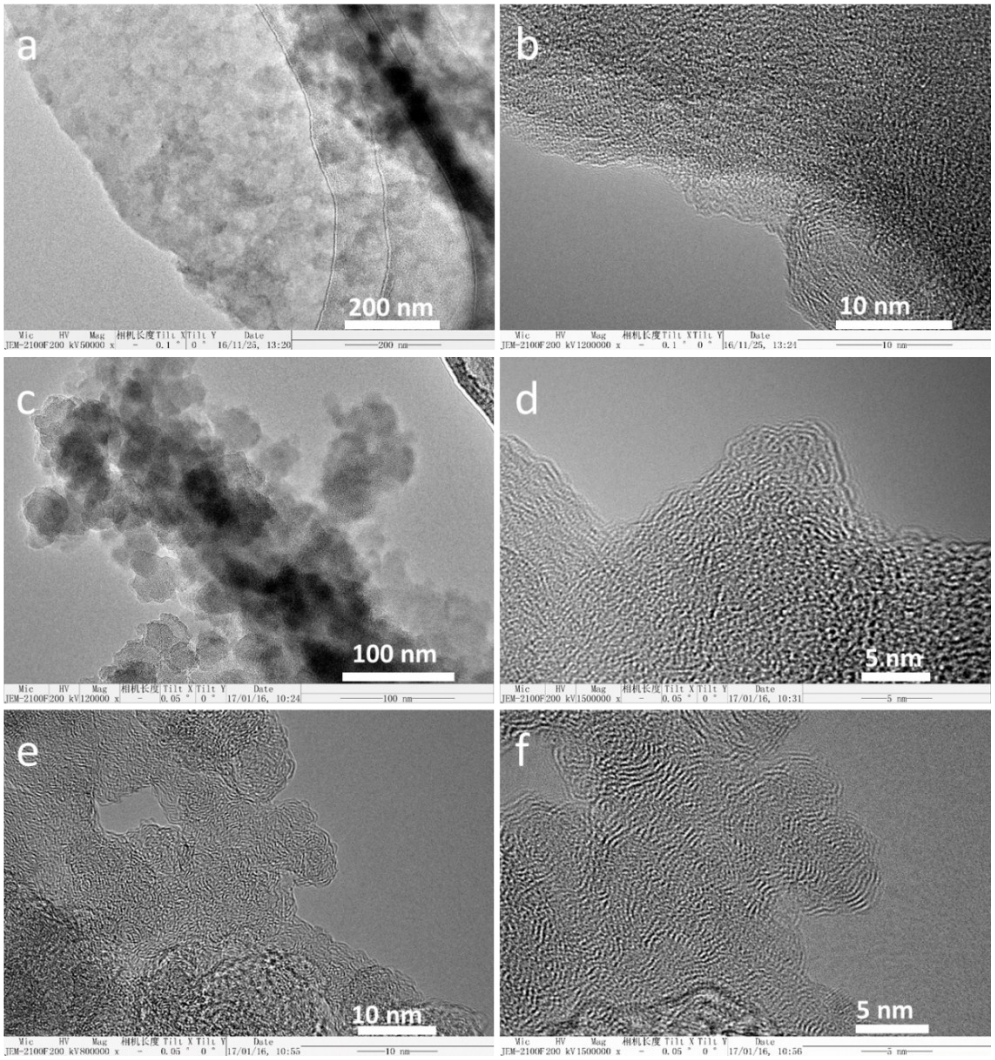

Figure S11. Structural stability of 2D nanoribbon (a, and b), 3D framework (c, and d) and 1D nanochain (e, and f).

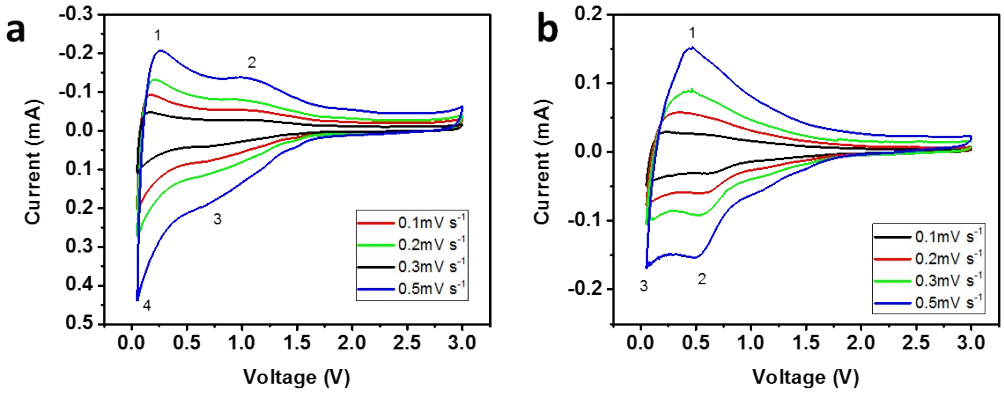

Figure S12. CV curves at different scanning rate of the GDY nanochain for storing a) Li-ion and b) Na-ion.

Reference

1 Hong, G. *et al.* Direct Growth of Semiconducting Single-Walled Carbon Nanotube Array. *Journal of the American Chemical Society* **131**, 14642-14643, doi:10.1021/ja9068529 (2009).

2 Li, X. S. *et al.* Large-Area Synthesis of High-Quality and Uniform Graphene Films on Copper Foils. *Science* **324**, 1312-1314, doi:10.1126/science.1171245 (2009).

3 Shi, L. *et al.* Scalable Seashell-Based Chemical Vapor Deposition Growth of Three-Dimensional Graphene Foams for Oil–Water Separation. *Journal of the American Chemical Society* **138**, 6360-6363, doi:10.1021/jacs.6b02262 (2016).

4 Wang, T.-S. *et al.* Russian-Doll-Type Metal Carbide Endofullerene: Synthesis, Isolation, and Characterization of Sc4C2@C80. *Journal of the American Chemical Society* **131**, 16646-16647, doi:10.1021/ja9077842 (2009).

5 Li, X. H. & Antonietti, M. Metal nanoparticles at mesoporous N-doped carbons and carbon nitrides: functional Mott-Schottky heterojunctions for catalysis. *Chem Soc Rev* **42**, 6593-6604, doi:10.1039/c3cs60067j (2013).

6 Zhao, X. *et al.* Incorporation of Manganese Dioxide within Ultraporous Activated Graphene for High-Performance Electrochemical Capacitors. *ACS Nano* **6**, 5404-5412, doi:10.1021/nn3012916 (2012).

7 Bianconi, P. A. *et al.* Diamond and Diamond-Like Carbon from a Preceramic Polymer. *Journal of the American Chemical Society* **126**, 3191-3202, doi:10.1021/ja039254l (2004).

8 Strong, H. M. & Chrenko, R. M. Diamond growth rates and physical properties of laboratory-made diamond. *The Journal of Physical Chemistry* **75**, 1838-1843, doi:10.1021/j100681a014 (1971).

9 Chen, L.-F. *et al.* Synthesis of Nitrogen-Doped Porous Carbon Nanofibers as an Efficient Electrode Material for Supercapacitors. *ACS Nano* **6**, 7092-7102, doi:10.1021/nn302147s (2012).

10 Wei, L., Sevilla, M., Fuertes, A. B., Mokaya, R. & Yushin, G. Polypyrrole-Derived Activated Carbons for High-Performance Electrical Double-Layer Capacitors with Ionic Liquid Electrolyte. *Adv Fun Mater* **22**, 827-834, doi:10.1002/adfm.201101866 (2012).

11 Ning, G. *et al.* High capacity gas storage in corrugated porous graphene with a specific surface area-lossless tightly stacking manner. *Chemical Communications* **48**, 6815-6817 (2012).

12 Butenko, Y. V. *et al.* Photoemission study of onionlike carbons produced by annealing nanodiamonds. *Physical Review B* **71**, doi:10.1103/PhysRevB.71.075420 (2005).

13 Georgakilas, V., Perman, J. A., Tucek, J. & Zboril, R. Broad Family of Carbon Nanoallotropes: Classification, Chemistry, and Applications of Fullerenes, Carbon Dots, Nanotubes, Graphene, Nanodiamonds, and Combined Superstructures. *Chemical Reviews* **115**, 4744-4822, doi:10.1021/cr500304f (2015).